Signal Processing 93 (2013) 3504–3514

Contents lists available at ScienceDirect

Signal Processing

journal homepage: www.elsevier.com/locate/sigpro

Wideband source localization using sparse learning via iterative minimization

Luzhou Xu [a], Kexin Zhao [a], Jian Li [a,*], Petre Stoica [b]

[a] Department of Electrical and Computer Engineering, University of Florida, Gainesville, FL 32611-6130, USA
[b] Department of Information Technology, Uppsala University, SE-75105 Uppsala, Sweden

ARTICLE INFO

Article history:
Received 2 August 2012
Received in revised form
26 March 2013
Accepted 2 April 2013
Available online 12 April 2013

Dedicated to the memory of Professor Alex B. Gershman (1962–2011)

Keywords:
Wideband source localization
Sparse signal recovery
Vector sensor array
Sparse learning via iterative minimization (SLIM)

ABSTRACT

In this paper, two extensions of the Sparse Learning via Iterative Minimization (SLIM) algorithm are presented for wideband source localization using a sensor array. The proposed methods exploit the joint sparse structure across all frequency bins, and estimate the spatial pseudo-spectra at various frequency bins jointly and iteratively. Via several numerical examples, we show that the proposed methods can provide high-resolution angle estimates and excellent source localization performance, and are able to resolve the left–right ambiguity problem, when used together with the vector sensor array technology.

1. Introduction

Source localization using a sensor array plays an important role in a large variety of signal processing applications involving electromagnetic, acoustic, and seismic sensing. Many advanced source localization techniques, such as MUSIC, Capon, and ESPRIT (see [1] and references therein), have been developed in the past decades. However, most algorithms in the literature were developed under the narrowband assumption, under which the time-difference of arrival (TDOA) of a signal at various sensors is negligible. In other words, it is assumed that a signal arrives at various sensors simultaneously with different phase shifts. However, in many practical applications, such as aeroacoustic array processing [2] and sonar [3,4], this assumption is not valid, and the challenging wideband array processing problem arises.

Several adaptive wideband source localization approaches, including the spatial-time–frequency-distribution based method (e.g., [5]) and the focussing-matrix based coherent signal-subspace (CSS) method (e.g., [6]), have been developed in the literature. However, the former is proposed for angle estimation in the particular case of chirp sources, while for the latter the requirement of preliminary angle estimates and the need for the design of a focusing matrix for each frequency bin are rather complicated tasks.

On the other hand, the sparse signal recovery (SSR) techniques have attracted much interest among researchers recently (e.g., [7–9]). Sparse algorithms, such as ℓ_1 norm minimization (e.g., [8,10]) and FOCal Underdetermined System Solution (FOCUSS) [9], have been applied to the narrowband source localization problem, resulting in better localization performance and enhanced capability of resolving closely spaced sources [9–11]. Among the numerous adaptive SSR algorithms, the recently developed

* Corresponding author. Tel.: +1 352 392 2642; fax: +1 352 392 0044.
E-mail address: li@dsp.ufl.edu (J. Li).

0165-1684/$ - see front matter © 2013 Elsevier B.V. All rights reserved.
http://dx.doi.org/10.1016/j.sigpro.2013.04.005

user-parameter free Sparse Learning via Iterative Minimization (SLIM) algorithm [12,13] has shown satisfactory performances in various applications, such as nonparametric spectral estimation, radar imaging, and channel estimation for underwater acoustic communications [12]. The SLIM algorithm can work with even a single snapshot, arbitrary array geometry, coherent or non-coherent sources, and offers high resolution spatial estimation results at a relatively low computational complexity [12].

To reap the SSR benefits, several SSR-based wideband source localization methods have been developed. In [14], the authors formulate the wideband source localization problem as a joint/group sparsity problem, and then propose a modified CoSaMP [15] method to solve the joint sparse signal recovery problem. However, it is known that CoSaMP and its orthogonal matching pursuit (OMP) variations fail to provide satisfactory performance in the source localization and spectral estimation applications, especially in the presence of closely spaced sources (see, e.g., [16]). A method, named wideband covariance matrix sparse representation (W-CMSR), is proposed in [17], by using the covariance matrix fitting technique. This method requires a priori information on the source correlation functions, which is not available in many practical applications, such as aeroacoustic and passive sonar.

The group LASSO (gLASSO) algorithm [18] can also be applied to the wideband source localization problem. As the conventional LASSO algorithm, gLASSO contains a user parameter balancing the fitting error and the sparsity promoting term. Selecting this user parameter is a difficult task. Furthermore, in [18] the shooting algorithm [19] is utilized to solve the gLASSO optimization problem, which essentially minimizes the cost function with respect to various groups of coefficients cyclically. As we will show via numerical examples, this algorithm suffers from a slow convergence problem, and fails to provide satisfactory results. We further remark that many theoretical analyses of gLASSO have been performed in the literature [20,21] to investigate its uniqueness and recovery conditions. However, most of their conditions are not satisfied in the source localization applications, where steering vectors could be highly correlated to each other depending on the selected angle searching granularity. To our best knowledge, it is still an open problem to theoretically analyze the behavior and performance of gLASSO, as well as many other SSR algorithms, when the base vectors are sampled from a continuous manifold function.

In this paper, we present two extensions of the SLIM algorithm in [12,13] to wideband source localization, referred to as WB-SLIM-0 and WB-SLIM-1. Both algorithms exploit the joint/group sparse structure. We consider wideband sources which emit wideband signals occupying all frequencies of interest. Hence, once we find a signal at a certain angle and a specific frequency, we can expect signals at the same angle and other frequencies. To exploit the joint spatial sparse structure, we utilize a hierarchical Bayesian model and assume the same statistical distribution of spatial pseudo-spectra for various frequencies. The cyclic minimization (CM) approach [22] is then used to solve the Maximum a Posteriori (MAP) problem. As we will discuss in Section 3.3, the WB-SLIM-1 algorithm can be also formulated in a similar form as gLASSO. However, unlike the existing gLASSO algorithm, WB-SLIM-1 is user parameter free and hence does not require fine tuning of user-parameter(s). Moreover, the proposed algorithm can converge much faster than the existing gLASSO algorithms [18].

We demonstrate the effectiveness of the proposed WB-SLIM algorithms for acoustic source localization using both the acoustic vector sensor arrays (VSA) [23–25] and the conventional scalar sensor arrays (SSA). Acoustic vector sensors measure scalar pressure along with particle motion, and have attracted much attention from researchers and practitioners alike. This technology features many advantages over the omnidirectional hydrophone sensor, including resolving of spatial left–right ambiguity and the ability to "undersample" an acoustic wave without spatial aliasing. However, we have noticed that due to the wide beam of a single vector sensor, the ambiguity lobe cannot be eliminated effectively using the conventional data-independent delay-and-sum (DAS) approach, especially when the steering angle is near endfire. This fact implies that DAS cannot detect and localize targets near endfire uniquely, even with a vector sensor array. In this paper, we will demonstrate that the proposed WB-SLIM algorithms, along with VSA, can effectively resolve the left–right ambiguity problem.

Notation: We denote vectors and matrices by boldface lowercase and boldface uppercase letters, respectively. Table 1 specifies the symbols, used in the paper, and their meanings.

2. Data model

Consider K far-field wideband source signals arriving at a sensor array from directions $\{\theta_k\}_{k=1}^{K}$. Let L be the number of samples of the received signal. At the pre-processing stage, an L-point discrete Fourier transform (DFT) is applied to the time-domain data received at each sensor to convert the wideband signal into L narrowband frequency signals. Then, the array output vector $\{\mathbf{y}_l\}$ in the presence of additive noise can be represented as (see, e.g., [6,14])

$$\mathbf{y}_l = \sum_{k=1}^{K} \mathbf{a}_l(\theta_k) x_{k,l} + \mathbf{n}_l \quad \text{for } l = 1, 2, \ldots, L \tag{1}$$

where $\mathbf{a}_l(\theta_k)$ is the $M \times 1$ steering vector for the signal arriving from θ_k at the lth frequency bin, with f_l as the center frequency, and M is the number of sensors. Specifically, for a uniform linear array (ULA) formed by scalar

Table 1
Notation used in the text.

$\triangleq$	A definition
$\|\cdot\|$	Euclidean norm
$\odot$	The Hadamard (elementwise) matrix product
$\otimes$	The Kronecker matrix product
$(\cdot)^T$	Transpose of a vector or matrix
$(\cdot)^H$	Conjugate transpose of a vector or matrix
Diag$(\cdot)$	Diagonal matrix with the argument vector on its diagonal
Re$\{\cdot\}$	The real part of a scalar, vector or matrix
$\mathbf{I}$	Identity matrix of appropriate dimension

sensors with inter-element spacing δ, the steering vector can be written as

$$\mathbf{a}_l(\theta_k)=[1 \;\; e^{-j2\pi(f_l\delta\cos(\theta_k)/c)} \;\; e^{-j4\pi(f_l\delta\cos(\theta_k)/c)} \;\; \ldots \;\; e^{-j2(M-1)\pi f_l\delta\cos(\theta_k)/c}]^T, \tag{2}$$

where c denotes the propagation speed, and θ_k is defined relative to the endfire. For a vector sensor array (e.g., [23–25]), $\mathbf{a}_l(\theta_k)$ can be written as

$$\mathbf{a}_l(\theta_k)=\mathbf{a}_{l,\text{array}}(\theta_k)\otimes\mathbf{a}_{\text{VS}}, \tag{3}$$

where $\mathbf{a}_{l,\text{array}}$ is the array steering vector for a scalar sensor array with an equivalent spatial configuration and plane wave input, $\mathbf{a}_{\text{VS}}$ denotes the response of a single vector sensor (see [25]), and $\otimes$ denotes the matrix Kronecker product. In (1), $x_{k,l}$ denotes the complex-valued amplitude of the signal arriving from θ_k at the lth frequency bin, and $\mathbf{n}_l$ denotes the noise and interference.

In practice, the number of wideband sources K is usually unknown. We use a fine angle grid, denoted by $\{\theta_n\}_{n=1}^N$, covering the set of locations of sources. Each point of this grid is considered to be a potential source location. Via estimating the signal power arriving at each potential angle, we obtain spatial pseudo-spectra for various frequency bins, from which the sources can be detected and localized. Therefore, the following SSR problem arises:

$$\mathbf{y}_l=\mathbf{A}_l\mathbf{x}_l+\mathbf{n}_l, \quad l=1,\ldots,L, \tag{4}$$

where $\mathbf{A}_l=[\mathbf{a}_l(\theta_1),\ldots,\mathbf{a}_l(\theta_N)]\in\mathbb{C}^{M\times N}$ with $\mathbf{a}_l(\theta_n)$ denoting the steering vector for the nth point of the scanning grid at the lth frequency bin, $\mathbf{x}_l=[x_{1,l},x_{2,l},\ldots,x_{N,l}]^T\in\mathbb{C}^{N\times 1}$ denotes the pseudo-spatial spectrum at the grid points and the lth frequency bin. Note that usually $N\gg K$. Hence, the columns of $\mathbf{A}_l$ form an overcomplete basis for the signal $\mathbf{y}_l$. Generally, $\mathbf{x}_l$ cannot be determined uniquely from (4). However, in real applications, the number of sources is relatively small. This leads to a sparse property of $\mathbf{x}_l$ that can be exploited to identify $\mathbf{x}_l$ uniquely.

Note that the data model in (4) is different from the multi-snapshot model in [11,26], where the steering matrices are the same for all snapshots, i.e., $\mathbf{A}_1=\mathbf{A}_2=\cdots=\mathbf{A}_L$. Note also that (4) can be re-written in the form of the standard SSR data model $\mathbf{y}=\mathbf{A}\mathbf{x}+\mathbf{n}$ by stacking the column vectors $\{\mathbf{y}_l\}$ on top of each other and with the steering matrix $\mathbf{A}$ being a block-diagonal matrix formed by $\{\mathbf{A}_l\}$. The group/block SSR techniques [27,28] can then be applied. However, most of the existing group/block SSR algorithms, such as gLASSO [18], are formulated using the regularization technique, which requires fine tuning of user-parameter(s).

3. The wideband SLIM algorithms

Inspired by the SLIM algorithm in [12,13], we present in this section two algorithms, referred to as WB-SLIM-0 and WB-SLIM-1.

3.1. WB-SLIM-0

To exploit the aforementioned sparsity structure, we utilize the hierarchical Bayesian model [29]. First, we assume that the noise vectors $\{\mathbf{n}_l\}$ are independently identically distributed (i.i.d.) circularly symmetric complex Gaussian random vectors with zero mean and covariance matrix $\eta\mathbf{I}$ with η being an unknown deterministic parameter. We further assume $\{\mathbf{x}_l\}$ to be i.i.d. circularly symmetric complex Gaussian random vectors with zero mean and a diagonal covariance matrix $\mathbf{P}\triangleq\text{Diag}\{p_1,p_2,\ldots,p_N\}$. In this subsection, $\{p_n\}$ are assumed to be deterministic unknowns. Note that the joint sparsity structure of $\{\mathbf{x}_l\}$ across frequency bins is imposed via assuming the same covariance matrix $\mathbf{P}$ for all $\{\mathbf{x}_l\}$.

From the above assumptions, we have the following probability density functions (pdf):

$$f(\{\mathbf{y}_l\}|\{\mathbf{x}_l\},\eta)=\prod_{l=1}^{L}f(\mathbf{y}_l|\mathbf{x}_l,\eta)=\prod_{l=1}^{L}\frac{1}{(\pi\eta)^M}e^{-(1/\eta)\|\mathbf{y}_l-\mathbf{A}_l\mathbf{x}_l\|^2}, \tag{5}$$

and

$$f(\{\mathbf{x}_l\}|\{p_n\})=\prod_{l=1}^{L}\frac{1}{\pi^N\prod_{n=1}^{N}p_n}e^{-\mathbf{x}_l^H\mathbf{P}^{-1}\mathbf{x}_l}. \tag{6}$$

The WB-SLIM-0 estimates of $\{\mathbf{x}_l\}$, $\{p_n\}$ and η are obtained by solving the following maximum a posteriori (MAP) problem:

$$\min_{\{\mathbf{x}_l\}\{p_n\},\eta} g_{\text{WB-SLIM-0}}(\{\mathbf{x}_l\}\{p_n\},\eta), \tag{7}$$

where

$$g_{\text{WB-SLIM-0}}\triangleq-\log[f(\{\mathbf{y}_l\}|\{\mathbf{x}_l\},\eta)f(\{\mathbf{x}_l\}|\{p_n\})]. \tag{8}$$

From (5), (6) and after discarding irrelevant constants, $g_{\text{WB-SLIM-0}}$ can be expressed as

$$g_{\text{WB-SLIM-0}}=LM\log\eta+\frac{1}{\eta}\sum_{l=1}^{L}\|\mathbf{y}_l-\mathbf{A}_l\mathbf{x}_l\|^2 + L\sum_{n=1}^{N}\log p_n+\sum_{l=1}^{L}\sum_{n=1}^{N}\frac{|x_{n,l}|^2}{p_n}. \tag{9}$$

Note that when $p_n\to 0$ or $\eta\to 0$, the cost function in (9) can approach $-\infty$ for certain values of $\{\mathbf{x}_l\}$. In other words, this cost function does not have a global minimum over the unconstrained parameter set. To address this problem, we constrain $p_n\geq\epsilon$ and $\eta\geq\epsilon$, with ϵ being a small positive number ($\epsilon=10^{-16}$ in our numerical examples). We remark that under the constraint that $p_n\geq\epsilon$, minimizing (9) will not lead to a strictly sparse solution, i.e., p_n, as well as elements of $\mathbf{x}_l$, will not be exactly zeros. However, as we will show via numerical examples, the so-obtained solution can be considered sparse practically, in the sense that most of the obtained $\{p_n\}$ are much smaller than the rest and hence the sources can be easily separated from noise.

The optimization problem of (7) can be solved by using the cyclic minimization (CM) technique [22]. First, given $\{\mathbf{x}_l\}_{l=1}^L$ and η, the minimization problem can be decoupled and simplified as follows:

$$\min_{p_n} \quad g_n(p_n)\triangleq L\log p_n+\frac{\sum_{l=1}^{L}|x_{n,l}|^2}{p_n} \quad \text{s.t. } p_n\geq\epsilon, \tag{10}$$

for $n=1,2,\ldots,N$. Differentiating $g_n(p_n)$ with respect to (w.r.t.) p_n yields

$$\frac{\partial g_n(p_n)}{\partial p_n}=\frac{L}{p_n}-\frac{1}{p_n^2}\sum_{l=1}^{L}|x_{n,l}|^2. \tag{11}$$

We can easily verify that $\partial g_n(p_n)/\partial p_n=0$ when

Table 2
WB-SLIM algorithms.

Initialize $\{\mathbf{x}_l\}_{l=1}^L$ and η with the DAS estimates as follows:

$$\mathbf{x}_{n,l}^{(0)} = \mathbf{a}_l^H(\theta_n)\mathbf{y}_l/\|\mathbf{a}_l(\theta_n)\|^2, \quad \text{for } n=1,\ldots,N;\ \ l=1,\ldots,L;$$

$$\eta^{(0)} = \max\left\{\frac{1}{10LM}\sum_{l=1}^L\|\mathbf{x}_l^{(0)}\|^2, \epsilon\right\}$$

Repeat the following steps for $t=0,1,2,\ldots$:

$$p_n^{(t+1)} = \begin{cases} \max\left\{\frac{1}{L}\sum_{l=1}^L |x_{n,l}^{(t)}|^2, \epsilon\right\} & (\text{WB}-\text{SLIM}-0) \\ \max\left\{\sqrt{\frac{1}{L}\sum_{l=1}^L |x_{n,l}^{(t)}|^2}, \epsilon\right\} & (\text{WB}-\text{SLIM}-1) \end{cases}, \quad \text{for } n=1,\ldots,N;$$

$$\mathbf{x}_l^{(t+1)} = \mathbf{P}^{(t+1)}\mathbf{A}_l^H(\mathbf{A}_l\mathbf{P}^{(t+1)}\mathbf{A}_l^H + \eta^{(t)}\mathbf{I})^{-1}\mathbf{y}_l, \quad l=1,\ldots,L;$$

$$\eta^{(t+1)} = \max\left\{\frac{1}{LM}\sum_{l=1}^L\|\mathbf{y}_l - \mathbf{A}_l\mathbf{x}_l^{(t+1)}\|^2, \epsilon\right\}.$$

until convergence

$p_n = (1/L)\sum_{l=1}^L |x_{n,l}|^2$. Furthermore, the cost function $g_n(p_n)$ is monotonically decreasing when $0 < p_n \le (1/L)\sum_{l=1}^L |x_{n,l}|^2$, and monotonically increasing when $p_n \ge (1/L)\sum_{l=1}^L |x_{n,l}|^2$. Therefore, the optimal solution of (10) is

$$p_n = \max\left\{\frac{1}{L}\sum_{l=1}^L |x_{n,l}|^2, \epsilon\right\}, \quad n=1,\ldots,N. \tag{12}$$

Similarly, given $\{\mathbf{x}_l\}_{l=1}^L$ and $\{p_n\}$, the optimization problem reduces to

$$\min_{\eta} \quad g(\eta) \triangleq LM\log\eta + \frac{1}{\eta}\sum_{l=1}^L\|\mathbf{y}_l - \mathbf{A}_l\mathbf{x}_l\|^2 \quad \text{s.t. } \eta \ge \epsilon, \tag{13}$$

whose solution can be obtained easily as follows:

$$\eta = \max\left\{\frac{1}{LM}\sum_{l=1}^L\|\mathbf{y}_l - \mathbf{A}_l\mathbf{x}_l\|^2, \epsilon\right\}. \tag{14}$$

Finally, for given η and p_n, differentiating $g_{\text{WB-SLIM-0}}$ w.r.t. $\mathbf{x}_l$ and setting the derivative to zero yield

$$\begin{aligned}\mathbf{x}_l &= [\mathbf{A}_l^H\mathbf{A}_l + \eta\mathbf{P}^{-1}]^{-1}\mathbf{A}_l^H\mathbf{y}_l \\ &= \mathbf{P}\mathbf{A}_l^H[\mathbf{A}_l\mathbf{P}\mathbf{A}_l^H + \eta\mathbf{I}]^{-1}\mathbf{y}_l, \quad l=1,\ldots,L.\end{aligned} \tag{15}$$

The solution of (7) can be obtained via iterating (12), (14) and (15).

3.2. WB-SLIM-1

As we will show by numerical examples, WB-SLIM-0 provides a sparse solution. However, the downside of this is that it may fail to detect weak targets, especially at low SNR. In this subsection, we propose a variation of WB-SLIM-0, called WB-SLIM-1, which provides a less sparse but more robust solution.

In addition to the Gaussian distribution assumptions on $\{\mathbf{n}_l\}$ and $\{\mathbf{x}_l\}$ introduced in Section 3.1, we further assume that $\{p_n\}_{n=1}^N$ are i.i.d. Gamma $(L+1, 1/L)$ distributed that is

$$f(p_n) \propto p_n^L e^{-Lp_n}, \quad n=1,\ldots,N. \tag{16}$$

Similarly to WB-SLIM-0, after taking the negative logarithm of the joint pdf, we obtain the cost function:

$$g_{\text{WB-SLIM-1}} = LM\log\eta + \frac{1}{\eta}\sum_{l=1}^L\|\mathbf{y}_l - \mathbf{A}_l\mathbf{x}_l\|^2 + L\sum_{n=1}^N p_n + \sum_{l=1}^L\sum_{n=1}^N\frac{|x_{n,l}|^2}{p_n}. \tag{17}$$

We apply a similar cyclic optimization procedure to (17), as detailed below. For fixed $\{\mathbf{x}_l\}$ and η, the optimization problem reduces to

$$\min_{p_n} \quad Lp_n + \sum_{l=1}^L\frac{|x_{n,l}|^2}{p_n} \quad \text{s.t. } p_n \ge \epsilon. \tag{18}$$

By using the same technique as for (12), we can easily get the optimal solution for (18) as follows:

$$p_n = \max\left\{\sqrt{\frac{1}{L}\sum_{l=1}^L |x_{n,l}|^2}, \epsilon\right\} \quad \text{for } n=1,\ldots,N. \tag{19}$$

The updating of $\mathbf{x}_l$ and η is exactly the same as for WB-SLIM-0 (see (15) and (14)).

3.3. Discussion

The WB-SLIM-0 and WB-SLIM-1 algorithms are summarized in Table 2. Both algorithms are initialized using the conventional delay-and-sum (DAS) estimates.

As shown in Table 2, the difference between WB-SLIM-0 and WB-SLIM-1 lies in the $\{p_n\}$ updates, due to the different *priors* assumed for $\{p_n\}$. We remark on the fact that under the constraints $\eta \ge \epsilon$ and $p_n \ge \epsilon$ for $n=1,\ldots,N$, the cost functions of WB-SLIM-0 and WB-SLIM-1 in (9) and (17) are bounded from below. By a cyclic minimization (CM) property, the cost functions are monotonically non-increasing at each iteration. This implies that both WB-SLIM-1 and WB-SLIM-0 are convergent in terms of cost function. Our empirical experience suggests that the proposed WB-SLIM algorithms do not provide significant performance improvements after about 20 iterations. We further remark that the cost function in (9) is not convex.

Hence, convergence to the global optimum is not guaranteed for any algorithm, including those proposed ones. However, as we will demonstrate numerically, a good estimation result can be achieved via choosing the initialization appropriately.

Note also that ignoring the constraint $p_n \geq \epsilon$ and minimizing the cost functions (9) and (17) with respect to $\{\mathbf{p}_n\}$, the concentrated cost functions can be written (to within an additive constant), respectively, as follows:

$$g_{\text{WB-SLIM-0}} = LM \log \eta + \frac{1}{\eta} \sum_{l=1}^{L} \|\mathbf{y}_l - \mathbf{A}_l \mathbf{x}_l\|^2 + \sum_{n=1}^{N} \log \left[\sum_{l=1}^{L} |x_{n,l}|^2 \right], \tag{20}$$

and

$$g_{\text{WB-SLIM-1}} = LM \log \eta + \frac{1}{\eta} \sum_{l=1}^{L} \|\mathbf{y}_l - \mathbf{A}_l \mathbf{x}_l\|^2 + 2\sqrt{L} \sum_{n=1}^{N} \left[\sum_{l=1}^{L} |x_{n,l}|^2 \right]^{1/2}. \tag{21}$$

Therefore, the WB-SLIM-0 and WB-SLIM-1 algorithms can be reformulated as the minimization of (20) and (21), respectively, which are extensions of the SLIM-q formulation (with $q=0$ or 1) in [13]. The original cost functions (9) and (17) can be interpreted as augmented functions of (20) and (21), which introduce additional optimization variables (i.e., $\{p_n\}$) to facilitate the CM technique. This augmentation optimization technique can also be used to solve the gLASSO optimization problem, which yields an algorithm similar to WB-SLIM-1 (Table 2) but with fixed η. In our experience, this new gLASSO algorithm can converge much faster than the existing one in the literature [18], where the shooting algorithm is used.

4. RELAX

The parametric RELAX [30,31] algorithm is adopted here to obtain the refined angle and power estimates. The WB-SLIM algorithms produce sparse spatial angle estimates and are able to resolve closely spaced sources. Hence the number of sources can be reliably determined by a simple thresholding procedure or by order selection algorithms such as the Bayesian information criterion (BIC) [32]. The RELAX algorithm requires information on the number of sources but does not depend on the scanning grid that covers the region of possible source locations, and hence it can be used to refine the WB-SLIM estimates.

The RELAX algorithm can be formulated as a joint nonlinear least-square problem:

$$\min_{\{\theta_k, x_{k,l}\}} \sum_{l=1}^{L} \|\mathbf{y}_l - \sum_{k=1}^{\hat{K}} \mathbf{a}_l(\theta_k) x_{k,l}\|^2, \tag{22}$$

where $\hat{K}$ is the estimated number of sources. Initialized with the WB-SLIM results, RELAX solves the optimization problem (22) cyclically. To update the estimates of the kth source, we define

$$\tilde{\mathbf{y}}_{k,l} = \mathbf{y}_l - \sum_{i \neq k} \mathbf{a}_l(\hat{\theta}_i) \hat{x}_{i,l}, \tag{23}$$

where $\{\hat{\theta}_i, \hat{x}_{i,l}\}_{i \neq k}$ are the most recent estimates of the other sources. Then, the optimization problem is reduced to

$$\min_{\{\theta_k, x_{k,l}\}} \sum_{l=1}^{L} \|\tilde{\mathbf{y}}_{k,l} - \mathbf{a}_l(\theta_k) x_{k,l}\|^2. \tag{24}$$

Solving this optimization problem yields the DAS-type estimates:

$$\hat{\theta}_k = \underset{\theta_k}{\text{argmax}} \sum_{l=1}^{L} |\mathbf{a}_l^H(\theta_k) \tilde{\mathbf{y}}_{k,l}|^2, \tag{25}$$

and

$$\hat{x}_{k,l} = \frac{\mathbf{a}_l^H(\hat{\theta}_k) \tilde{\mathbf{y}}_{k,l}}{\|\mathbf{a}_l(\hat{\theta}_k)\|^2} \quad \text{for } l = 1, 2, \ldots, L. \tag{26}$$

The RELAX algorithm updates $\{\hat{\theta}_k, \hat{x}_{k,l}\}$ for all sources iteratively using (25) and (26). We terminate the iteration when the norm of the difference between two consecutive estimates falls below a predefined small threshold (10^{-4} in our numerical examples). The RELAX approach is summarized in Table 3.

Owing to the CM approach employed, the RELAX algorithm is locally convergent. Note that RELAX requires only 1D maximizations around the WB-SLIM estimates. This maximization operation can be efficiently implemented using derivative-free uphill search methods such as the Nelder–Mead algorithm [33], which is incorporated in the MATLAB optimization toolbox as the function "fminsearch".

5. Numerical examples

In this section, we present several numerical examples to demonstrate the excellent angle estimation performance of the proposed methods. We consider two closely spaced wideband sources located near the array endfire at 10.11° and 11.02°. We assume that the signals emitted by the two sources are statistically independent with flat power spectra ranging from −10 kHz to 10 kHz. A 128-point FFT is performed at the preprocessing stage to decompose the entire frequency band into $L=128$ narrow frequency bins. The SNRs of the two sources are 25 dB and 20 dB, respectively, unless otherwise specified. We assume that the speed of sound (in the sea) is 1530 m/s.

We first consider a 20-element scalar-sensor ULA with the inter-element spacing equal to $\delta = 3$ m. We apply the proposed WB-SLIM-0 and WB-SLIM-1 to the received

Table 3
The RELAX algorithm.

$\hat{K}$: Number of sources obtained from WB-SLIM
$\{\hat{\theta}_k\}_{k=1}^{\hat{K}}$: Locations of the sources obtained from WB-SLIM
$\{\hat{x}_{k,l}\}_{k=1,l=1}^{\hat{K},L}$: Corresponding waveforms obtained from WB-SLIM
repeat
  for $k = 1, \ldots, \hat{K}$
    $\tilde{\mathbf{y}}_{k,l} = \mathbf{y}_l - \sum_{i=1, i \neq k}^{\hat{K}} \mathbf{a}_l(\hat{\theta}_i) \hat{x}_{i,l}, \quad l = 1, \ldots, L$
    $\hat{\theta}_k = \text{argmax}_{\theta_k} \sum_{l=1}^{L} |\mathbf{a}_l^H(\theta_k) \tilde{\mathbf{y}}_{k,l}|^2$
    $\hat{x}_{k,l} = \frac{\mathbf{a}_l^H(\hat{\theta}_k) \tilde{\mathbf{y}}_{k,l}}{\|\mathbf{a}_l(\hat{\theta}_k)\|^2}, \quad l = 1, \ldots, L$
  end for
until (convergence)

signal. For comparison purposes, several conventional angle estimation algorithms, namely DAS, NB-SLIM-0 and NB-SLIM-1, are also considered. These methods apply the DAS or the narrowband SLIM algorithms of [12,13] to each frequency bin, and then combine the obtained spatial pseudo-spectra non-coherently. For all the algorithms in this section, the scanning grid is uniform with 0.25° increment between adjacent points. Throughout the paper, the iteration number of group LASSO is set to 5000, and the iteration numbers of NB-SLIM and WB-SLIM are fixed to 50.

Fig. 1 shows the spatial pseudo-spectra, i.e., $\{p_n\}_{n=1}^{N}$, obtained by various algorithms. The dashed lines indicate the true angles. From Fig. 1(a)–(f), we can see clearly that the scalar-sensor array suffers from the left–right ambiguity problem. Furthermore, we note that the data-independent DAS algorithm suffers from the low-resolution problem: it is unable to resolve the two closely spaced targets. Fig. 1(b) shows the spatial pseudo-spectra obtained by gLASSO, which represents the best results we got via fine tuning of the gLASSO user-parameter. As we can see, the gLASSO algorithm fails to detect the two sources correctly. Note that the shooting algorithm has been used to obtain Fig. 1(b). As we discussed above, the augmentation optimization technique can also be used to solve the gLASSO problem. This new gLASSO algorithm yields similar results as the WB-SLIM-1 in Fig. 1(e). The spatial pseudo-spectra of NB-SLIM-1 and NB-SLIM-0 are shown in Fig. 1(c) and (d), respectively. These two narrowband SLIM algorithms can (although only barely) resolve the two closely spaced targets. However, both provide noisy spatial pseudo-spectra, which may lead to high false detection rates. The reason for this is that both methods apply the narrowband SLIM algorithm to each frequency bin independently. When the frequency is larger than 510 Hz, the corresponding inter-element spacing is larger than half wavelength. The narrowband SLIM algorithm will then generate ambiguous lobes for frequency bins with frequency larger than 510 Hz. After the non-coherent combination of spatial pseudo-spectra, these ambiguous lobes become high sidelobes. In contrast, as shown in Fig. 1 (e) and (f), both WB-SLIM-0 and WB-SLIM-1 are able to effectively suppress these high sidelobes, provide clean and sparse spatial pseudo-spectra, and neatly resolve the two closely spaced sources. Note that WB-SLIM-0 performs better than WB-SLIM-1 in this example.

Fig. 2 corresponds to a vector sensor array example. The simulation parameters are exactly the same as those used to obtain Fig. 1, except that the scalar sensors are replaced by vector sensors. From Fig. 2(a) and (b), we can see that, once again, DAS and gLASSO cannot resolve the two closely spaced sources. The ambiguous lobe around −10° is about 0.3 dB lower than the mainlobe. This means that the vector sensor array in principle has the capability to resolve the left–right ambiguity problem. As we can see from Fig. 2(c) and (d), NB-SLIM-1 and NB-SLIM-0 suppress the ambiguous lobe even more to about 10 dB under main lobe. Fig. 2(e) and (d) shows that the proposed WB-SLIM-0 and WB-SLIM-1 algorithms outperform their narrowband counterparts significantly. Both are able to provide clean and sparse spatial pseudo-spectra, resolve the two closely spaced sources, and suppress the ambiguous lobes. We consider a more challenging example in Fig. 3, where the SNR of the second source is decreased to 0 dB, i.e., 25 dB lower than for the first one. The other simulation parameters are the same as those used in Fig. 2. For a better illustration, we show the zoomed-in spatial pseudo-spectra in the region [0, 20] degrees. As we can see, only WB-SLIM-1 is able to identify the two sources correctly in this challenging case.

Fig. 4 shows the performance improvement achieved by using the RELAX algorithm. The simulation parameters are the same as those used in Fig. 1. We first utilize the WB-SLIM-1 or WB-SLIM-0 algorithm to detect the number of sources and obtain initial angle and amplitude estimates, which are then refined using RELAX. In Fig. 4(a) and (b), the red circles indicate the true angles and powers of the sources, and the black stars show the RELAX estimates. For comparison purposes, we also show the spatial pseudo-spectra of DAS and WB-SLIM, whose peaks indicate the corresponding angle and power estimates. We display the angle and power estimates obtained in 20 Monte-Carlo runs. From Fig. 4(a) and (b), we see that RELAX effectively refines the angle and power estimates of WB-SLIM-1 or WB-SLIM-0, and obtains quite accurate estimates.

Finally, we demonstrate the performance of various algorithms in terms of the detection rate and the root-mean-squared-error (RMSE). For performance comparison purposes, we compute the wideband deterministic Cramer–Rao bound (CRB) for the angle estimates, which is given by [34], as follows:

$$\mathrm{CRB}(\theta)=\frac{\eta}{2}\left[\sum_{l=1}^{L}\mathrm{Re}\{(\dot{\mathbf{A}}_l^H\boldsymbol{\Pi}_{\mathbf{A}_l}^{\perp}\dot{\mathbf{A}}_l)\odot(\mathbf{x}_l\mathbf{x}_l^H)^T\}\right]^{-1} \tag{27}$$

where

$$\dot{\mathbf{A}}_l\triangleq\left[\left.\frac{\mathrm{d}\mathbf{a}_l(\theta)}{\mathrm{d}\theta}\right|_{\theta=\theta_1},\ldots,\left.\frac{\mathrm{d}\mathbf{a}_l(\theta)}{\mathrm{d}\theta}\right|_{\theta=\theta_K}\right], \tag{28}$$

and

$$\boldsymbol{\Pi}_{\mathbf{A}_l}^{\perp}\triangleq\mathbf{I}-\mathbf{A}_l(\mathbf{A}_l^H\mathbf{A}_l)^{-1}\mathbf{A}_l^H. \tag{29}$$

We consider the same array and wideband sources for Fig. 1. The x-axes of Fig. 5(a)–(c) show the SNR of the first source. The SNR of the second source is 5 dB smaller than that of the first. We perform 100 Monte-Carlo simulations. A Monte-Carlo trial is deemed failed when one or more sources are not detected or either of the DOA estimates is more than 0.5° away from the corresponding true value. The detection rate is defined as the ratio of the number of trials in which both sources are detected and localized correctly over the total trial number. From Fig. 5(a), we can see that both WB-SLIM-0 and WB-SLIM-1 achieve 100% detection rate when SNR is larger than or equal to 5 dB. However, at low SNR, WB-SLIM-1 outperforms WB-SLIM-0 significantly. Fig. 5(b) and (c) shows that RELAX, initialized by either WB-SLIM-1 or WB-SLIM-0, can achieve good estimation performance. Note that when SNR is less than 5 dB, the RMSE of the WB-SLIM-0 and RELAX estimates is not defined due to the detection failure. Hence, we only provide RMSE when SNR $\geq$5 dB for this algorithm. The

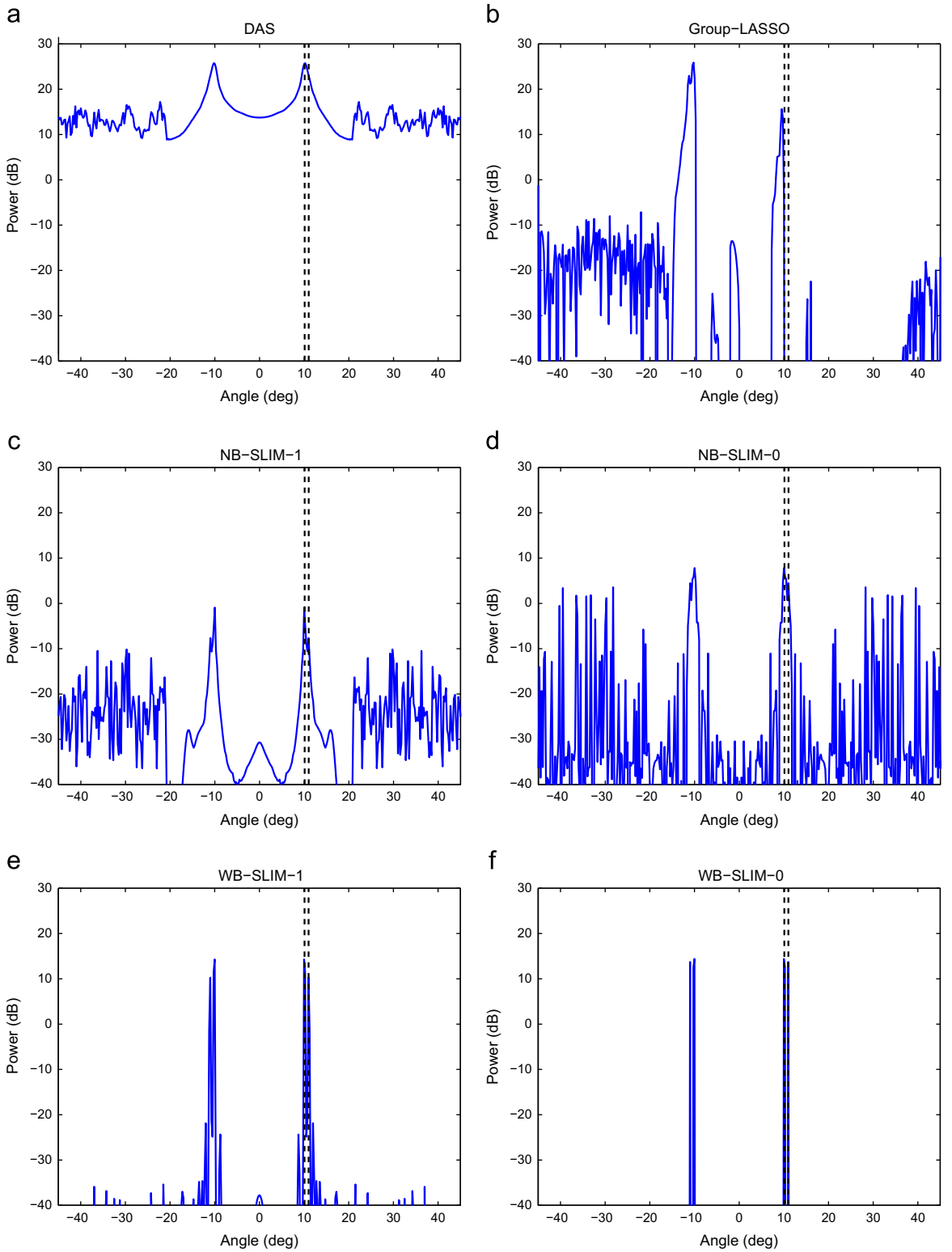

Fig. 1. Spatial pseudo-spectra obtained with a scalar sensor array and various algorithms: (a) DAS, (b) gLASSO, (c) NB-SLIM-1, (d) NB-SLIM-0, (e) WB-SLIM-1, and (f) WB-SLIM-0.

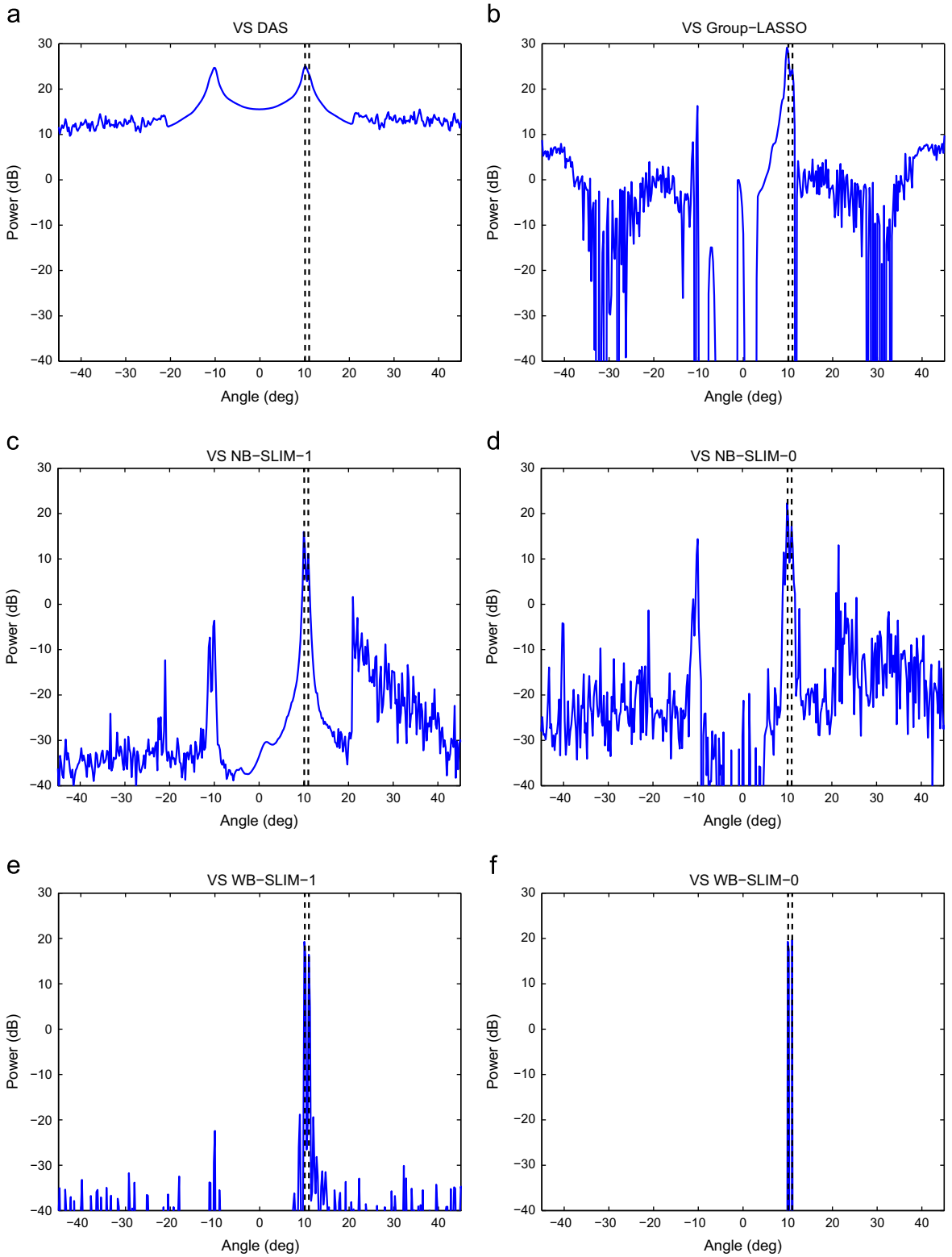

Fig. 2. Spatial pseudo-spectra obtained with a vector sensor array and various algorithms: (a) DAS, (b) gLASSO, (c) NB-SLIM-1, (d) NB-SLIM-0, (e) WB-SLIM-1, and (f) WB-SLIM-0.

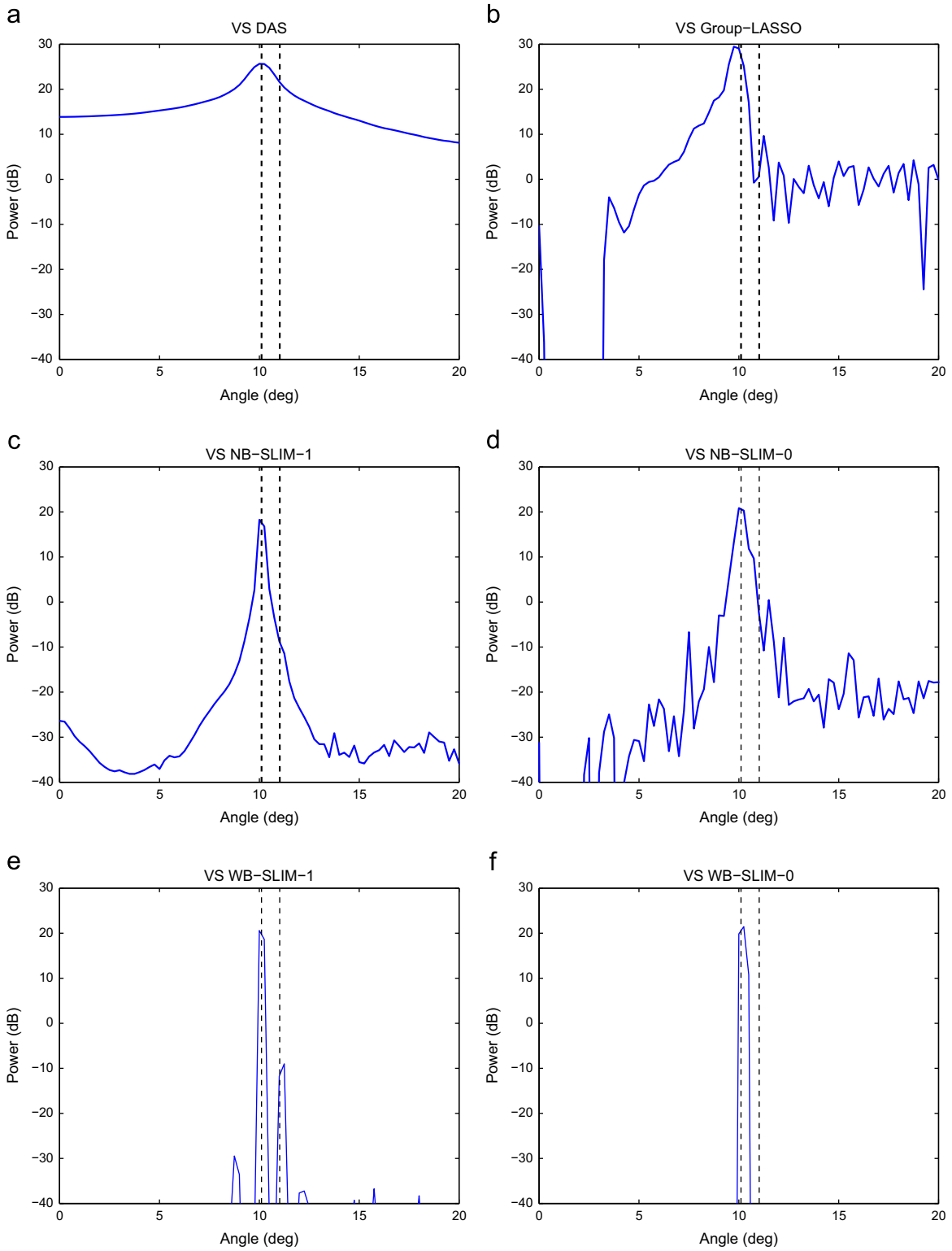

Fig. 3. Spatial pseudo-spectra, in the case of a weak source, obtained by various algorithms: (a) DAS, (b) gLASSO, (c) NB-SLIM-1, (d) NB-SLIM-0, (e) WB-SLIM-1, and (f) WB-SLIM-0.

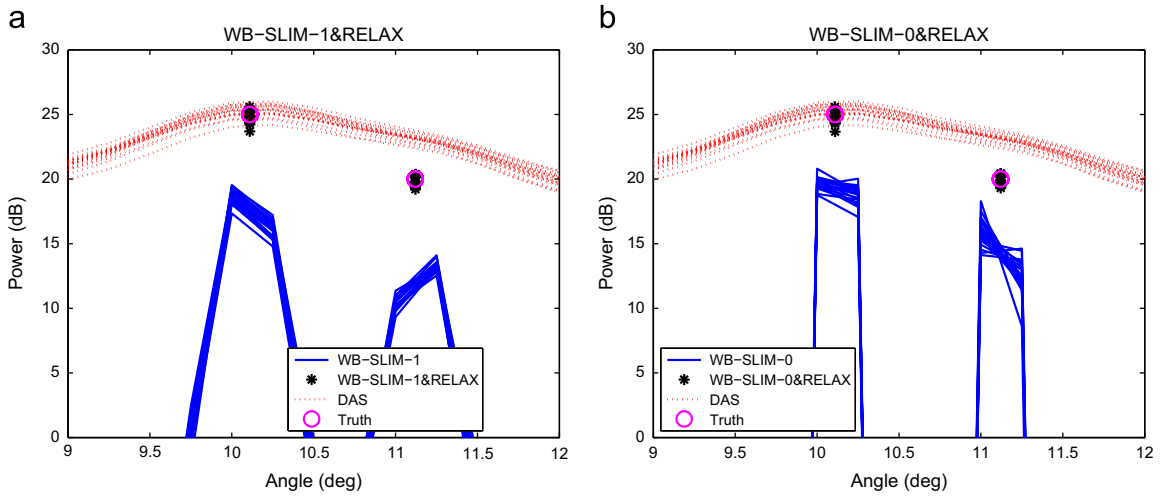

Fig. 4. Performance enhancement using RELAX. (a) WB-SLIM-1 and RELAX and (b) WB-SLIM-0 and RELAX. (For interpretation of the references to color in this figure caption, the reader is referred to the web version of this article.)

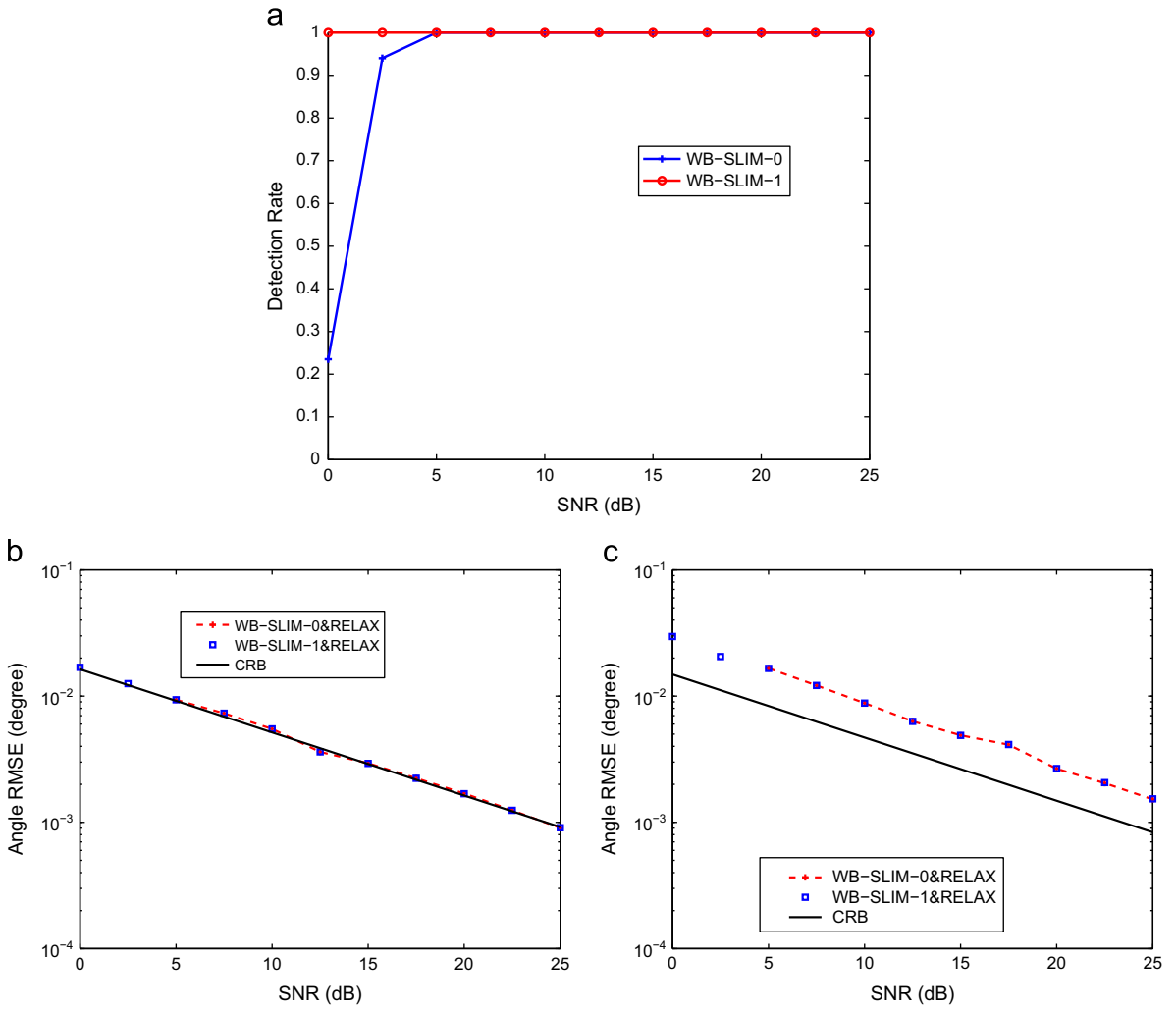

Fig. 5. Empirical failure rate and RMSEs versus SNR. (a) Detection rate, (b) RMSE of Source 1, and (c) RMSE of Source 2.

RMSEs of the angle estimates are approximately equal to RCRB for the stronger source, and are about two times the RCRB for the weak one (note that the deterministic CRB is not necessarily achievable, see, e.g., [34]).

6. Conclusions

Inspired by the narrowband SLIM algorithm, we have derived the WB-SLIM-0 and WB-SLIM-1 algorithms for wideband source localization, based on two different hierarchical Bayesian statistical models. These two algorithms provide high-resolution angle estimates without the need of tuning any user parameters, and are able to resolve the left–right ambiguity problem when used together with the vector sensor array technology. We have also proposed a wideband RELAX algorithm to refine the angle and power estimates obtained with WB-SLIM-0 and WB-SLIM-1 beyond the accuracy allowed by the fineness of the grid used in the latter. Several numerical examples have been provided to demonstrate the excellent source localization performance of the proposed methods.

Acknowledgments

This work was supported in part by the Office of Naval Research (ONR) under Grant no. N00014-12-1-0381, and the European Research Council (ERC). The helpful contributions of Qilin Zhang and Habti Abeida are acknowledged. We are also grateful to the editor, Prof. Nikos Sidiropoulos, and to three anonymous reviewers for providing us with a substantial number of detailed and helpful suggestions.

References

[1] H.L. Van Trees, Optimum Array Processing: Part IV of Detection, Estimation, and Modulation Theory, John Wiley & Sons, New York, NY, 2002.
[2] T. Yardibi, J. Li, P. Stoica, L.N. Cattafesta, Sparsity constrained deconvolution approaches for acoustic source mapping, The Journal of the Acoustical Society of America 123 (5) (2008) 2631–2642.
[3] A.B. Baggeroer, H. Cox, Passive sonar limits upon nulling multiple moving ships with large aperture arrays, in: 33th Asilomar Conference on Signals, Systems and Computers, vol. 1, 1999, pp. 103–108.
[4] A. Baggeroer, W. Kuperman, P. Mikhalevsky, An overview of matched field methods in ocean acoustics, IEEE Journal of Oceanic Engineering 18 (4) (1993) 401–424.
[5] A.B. Gershman, M.G. Amin, Wideband direction-of-arrival estimation of multiple chirp signals using spatial time–frequency distributions, IEEE Signal Processing Letters 7 (6) (2000) 152–155.
[6] H. Wang, M. Kaveh, Coherent signal-subspace processing for the detection and estimation of angles of arrival of multiple wide-band sources, IEEE Transactions on Acoustics, Speech, and Signal Processing ASSP-33 (4) (1985) 823–831.
[7] P. Stoica, P. Babu, J. Li, SPICE: a sparse covariance-based estimation method for array processing, IEEE Transactions on Signal Processing 59 (2) (2011) 629–638.
[8] D.L. Donoho, M. Elad, Optimally sparse representation in general nonorthogonal dictionaries via ℓ^1 minimization, Proceedings of the National Academy of Sciences of the United States of America 100 (5) (2003) 2197–2202.
[9] I.F. Gorodnitsky, B.D. Rao, Sparse signal reconstruction from limited data using FOCUSS: a re-weighted minimum norm algorithm, IEEE Transactions on Signal Processing 45 (3) (1997) 600–616.
[10] J.A. Tropp, Just relax: convex programming methods for identifying sparse signals, IEEE Transactions on Information Theory 51 (3) (2006) 1030–1051.
[11] D. Malioutov, M. Cetin, A. Willsky, A sparse signal reconstruction perspective for source localization with sensor arrays, IEEE Transactions on Signal Processing 53 (8) (2005) 3010–3022.
[12] J. Ling, X. Tan, T. Yardibi, J. Li, H. He, M.L. Nordenvaad, Enhanced channel estimation and efficient symbol detection in MIMO underwater acoustic communications, in: 43th Asilomar Conference on Signals, Systems and Computers, Pacific Grove, CA, 2009.
[13] X. Tan, W. Roberts, J. Li, P. Stoica, Sparse learning via iterative minimization with application to MIMO radar imaging, IEEE Transactions on Signal Processing 59 (3) (2011) 1088–1101.
[14] P.T. Boufounos, P. Smaragdis, B. Raj, Joint sparsity models for sideband array processing, in: M. Papadakis, D. Van De Ville, V.K. Goyal (Eds.), SPIE Wavelets and Sparsity XIV, San Diego, CA, USA, No. 9, 2011.
[15] D. Needell, J. Tropp, CoSaMP: iterative signal recovery from incomplete and inaccurate samples, Applied and Computational Harmonic Analysis 26 (2009) 301–321.
[16] D. Vu, L. Xu, M. Xue, J. Li, Nonparametric missing sample spectral analysis and its applications to interrupted SAR, IEEE Journal of Selected Topics in Signal Processing 6 (1) (2012) 1–14.
[17] Z.-M. Liu, Z.-T. Huang, Y.-Y. Zhou, Direction-of-arrival estimation of wideband signals via covariance matrix sparse representation, IEEE Transactions on Signal Processing 59 (9) (2011) 4256–4270.
[18] M. Yuan, Y. Lin, Model selection and estimation in regression with grouped variables, Journal of the Royal Statistical Society: Series B (Statistical Methodology) 68 (1) (2005) 49–67.
[19] W.J. Fu, Penalized regressions: the bridge versus the lasso, Journal of Computational and Graphical Statistics 7 (3) (1998) 397–416.
[20] F.R. Bach, Consistency of the group lasso and multiple kernel learning, The Journal of Machine Learning Research 9 (6) (2008) 1179–1225.
[21] X. Lv, G. Bi, C. Wan, The group lasso for stable recovery of block-sparse signal representations, IEEE Transactions on Signal Processing 59 (4) (2011) 1371–1381.
[22] P. Stoica, Y. Selén, Cyclic minimizers, majorization techniques, and expectation–maximization algorithm: a refresher, IEEE Signal Processing Magazine (2004) 112–114.
[23] A. Nehorai, E. Paldi, Acoustic vector-sensor array processing, IEEE Transactions on Signal Processing 42 (9) (1994) 2481–2491.
[24] M. Hawkes, A. Nehorai, Acoustic vector-sensor beamforming and Capon direction estimation, IEEE Transactions on Signal Processing 46 (9) (1998) 2291–2304.
[25] A.J. Poulsen, Robust Vector Sensor Array Processing and Performance Analysis, Ph.D. Dissertation, Massachusetts Institute of Technology, Boston, MA, 2009.
[26] M. Hyder, K. Mahata, Direction-of-arrival estimation using a mixed $l_{2,0}$ norm approximation, IEEE Transactions on Signal Processing 58 (9) (2010) 4646–4655.
[27] J. Huang, Structured Sparsity: Theorems, Algorithms and Applications, Ph.D. Dissertation, The State University of New Jersey, New Brunswick, NJ, 2011.
[28] Y.C. Eldar, P. Kuppinger, H. Bölcskei, Block-sparse signals: uncertainty relations and efficient recovery, IEEE Transactions on Signal Processing 58 (6) (2010) 3042–3054.
[29] M.E. Tipping, Sparse Bayesian learning and the relevance vector machine, Journal of Machine Learning Research 1 (2001) 211–244.
[30] J. Li, P. Stoica, Efficient mixed-spectrum estimation with applications to target feature extraction, IEEE Transactions on Signal Processing 44 (1996) 281–295.
[31] J. Li, P. Stoica, D. Zheng, Angle and waveform estimation via RELAX, IEEE Transactions on Aerospace and Electronic Systems 33 (1997) 1077–1087.
[32] G. Schwarz, Estimating the dimension of a model, The Annals of Statistics 6 (1978) 461–464.
[33] J.A. Nelder, R. Mead, A simplex method for function minimization, Computer Journal 7 (1965) 308–313.
[34] P. Stoica, A. Nehorai, MUSIC, maximum likelihood, and Cramer–Rao bound, IEEE Transactions on Acoustics, Speech, and Signal Processing ASSP-37 (5) (1989) 720–741.